Spatial structure of assimilated ozone in the upper troposphere and lower stratosphere

Krzysztof Wargan,[1,2,3] Steven Pawson,[1] Ivanka Stajner,[4] and Valérie Thouret[5,6]

Received 25 January 2010; revised 6 July 2010; accepted 14 September 2010; published 31 December 2010.

[1] Ozone distributions display a rich spatial structure in the upper troposphere and lower stratosphere (UTLS). This study uses in situ aircraft observations to examine how accurately such spatial distributions of ozone are represented in an assimilation of NASA's EOS-Aura ozone data using meteorological fields from the Goddard Earth Observing System, Version 4. Total ozone columns from the Ozone Monitoring Instrument (OMI) and stratospheric profiles from the Microwave Limb Sounder (MLS) are assimilated. The results demonstrate that the dominant large-scale ozone distribution is well-constrained (to realistic concentrations) near 250 hPa in the UTLS. Spatial patterns and the spectral power of variations are similar in the model simulations and the assimilation. The spectral power of the analysis increments is concentrated at large scales. Thus transport, rather than direct assimilation of small-scale features, is responsible for the spatial ozone structure in the UTLS. Consistent with the documented behavior of the Lin-Rood transport scheme, we demonstrate that the assimilated ozone represents realistic features on spatial scales of about four-to-six model grid boxes (500–800 km) and that smaller scales present in the aircraft observations are represented too weakly in the modeled and assimilated ozone fields. For the assimilated ozone, this result is robust over a range of realistic model-error-covariance length scales. The results indicate that observations of ozone on spatial scales that constrain the large-scale gradients are suited to producing global analyses of UTLS ozone that represent features at higher spatial resolution.

Citation: Wargan, K., S. Pawson, I. Stajner, and V. Thouret (2010), Spatial structure of assimilated ozone in the upper troposphere and lower stratosphere, *J. Geophys. Res.*, *115*, D24316, doi:10.1029/2010JD013941.

1. Introduction

[2] Ozone in the upper stratosphere and lower troposphere (UTLS) is known to provide important contributions to the planet's radiation balance and to shield the surface from potentially harmful ultraviolet radiation. Our knowledge of ozone distributions in the UTLS has historically been confined to localized information from sonde [e.g., *McPeters et al.*, 2007] and aircraft measurements [e.g., *Thouret et al.*, 1998], with contributions from occultation sensors in the past couple of decades [e.g., *Terao and Logan*, 2007]. The more recent availability of near-global satellite-based UTLS ozone profiles, with much higher spatiotemporal density than the historical networks, but with coarser vertical and horizontal resolution, provides opportunities for increased understanding of the UTLS ozone distribution. *Stajner et al.* [2008] and others have demonstrated that data assimilation systems can provide quite realistic representations of stratospheric ozone profiles and tropospheric ozone columns, when they ingest total ozone column and stratospheric profiles retrieved from satellite instrument measurements. This work extends *Stajner et al.* [2008] by examining the spatial structure of assimilated ozone in the UTLS.

[3] Previous studies have assessed assimilated ozone in the lower stratosphere and the UTLS. Space-based observations using nadir ultraviolet measurements, such as the Solar Backscattered Ultraviolet (SBUV) sensors, lose sensitivity to vertical ozone structure below about 64 hPa and consequently have little impact on UTLS profiles. Assimilation experiments using retrieved profiles from the Global Ozone Monitoring Experiment (GOME) [*de Laat et al.*, 2009] showed that even though UTLS ozone biases were corrected compared to chemistry-transport model (CTM) simulations, there was no positive impact on the structure of synoptic-scale ozone variations. Although very accurate, the sparse horizontal sampling of occultation measurements provides inadequate constraint for assimilation over most of the globe [e.g., *Stajner and Wargan*, 2004] unless additional mapping is performed [e.g., *Pierce et al.*, 2007].

[1]Global Modeling and Assimilation Office, NASA Goddard Space Flight Center, Greenbelt, Maryland, USA.
[2]Science Applications International Corporation, Beltsville, Maryland, USA.
[3]Now at Department of Physics, Imperial College London, London, UK.
[4]Noblis, Incorporated, Falls Church, Virginia, USA.
[5]Laboratoire d'Aérologie, UPS, Université de Toulouse, Toulouse, France.
[6]Laboratoire d'Aérologie, CNRS, Toulouse, France.

0148-0227/10/2010JD013941

The increasing availability of lower-stratospheric ozone information from successive limb-sounding instruments has led to increasingly realistic UTLS ozone profiles, compared to sonde observations, in the assimilated products [*Wargan et al.*, 2005; *Semane et al.*, 2007; *Jackson*, 2007; *Stajner et al.*, 2008; *Feng et al.*, 2008; *Parrington et al.*, 2008].

[4] The ozone assimilation system used here [*Stajner et al.*, 2008] incorporates retrieved total-column ozone from the Ozone Monitoring Instrument (OMI) [*Levelt et al.*, 2006; *McPeters et al.*, 2008] and ozone profiles, extending from the upper troposphere to the lower mesosphere, from the Microwave Limb Sounder (MLS) [*Froidevaux et al.*, 2006, 2008]. The assimilation merges these data with forecasts from an adapted version of the Goddard Earth Observing System, Version 4 (GEOS-4) general circulation model (GCM), which includes time-smoothed meteorological analyses [*Pawson et al.*, 2007] that are used to transport ozone and a linearized ozone chemistry module [*Stajner et al.*, 2008].

[5] This work provides a detailed evaluation of UTLS ozone in the GEOS assimilation system, focusing on the roles of physical versus statistical processes (transport versus assimilation) in defining the ozone structure. Following a description of the assimilation system, the analysis compares simulated to assimilated ozone structures (section 2) to evaluate the roles of transport and assimilation in determining spatial scales in the ozone fields. Evaluation of spatial structures in the assimilation and simulation against those observed by aircraft (section 3) then enables an assessment of the true resolution of the assimilated ozone fields: this impacts evaluation of the information content of assimilated ozone in the UTLS. Conclusions are presented in section 4.

2. Ozone Structure in the Model and Assimilation

2.1. System Descriptions

[6] Different components of the ozone model and assimilation system used in this work are described by *Bloom et al.* [2005], *Pawson et al.* [2007] and *Stajner et al.* [2008]. *Bloom et al.* [2005] give details of the GEOS-4 general circulation model (GCM) and the meteorological data assimilation system (DAS), which uses the Physical-space Statistical Analysis Scheme (PSAS). The system is run at 1° (latitude) × 1.25° (longitude) spatial resolution with 55 layers between the surface and about 80 km; nine layers lie between 300–70 hPa, producing a vertical resolution of 0.9–1.1 km near the tropopause. The GEOS-4 DAS includes meteorological data between the surface and about 55 km (0.4 hPa), using many types of in situ and space-based observations through the troposphere and stratosphere. *Pawson et al.* [2007] demonstrate that transport in GEOS-4 is substantially improved when 6 h time averaging is applied to the analyzed winds: the improvements were evident in simulated trace gas distributions and in the "observation-minus-forecast" (O-F) statistics of assimilated Solar Backscatter Ultra-Violet (SBUV) ozone fields.

[7] The model run performed for this study uses the time-smoothed meteorological analyses from GEOS-4. Photochemistry is approximated using a linearized ozone scheme [*Stajner et al.*, 2008], with prescribed photochemical production rates (P) and loss frequencies (L). Stratospheric P and L are adapted from zonal and monthly values by *Douglass et al.* [1996]. Daily values of tropospheric P and L are archived from the GEOS-CHEM model on a three-dimensional grid [*Hudman et al.*, 2007]. Note that in the UTLS, which is the focus of this paper, ozone chemistry is relatively slow and thus transport plays the dominant role in shaping the tracer fields.

[8] Two types of ozone data from EOS-Aura, OMI columns and MLS profiles, are included in the assimilation, with forecasts (background states) provided by the identical model (with identical meteorological fields) as the model simulation. The OMTO3 Collection 2 retrievals from OMI are based on the Total Ozone Mapping Spectrometer (TOMS) v8 total ozone algorithm [*Bhartia and Wellemeyer*, 2002]. These OMI OMTO3 ozone column retrievals have been compared extensively validated against an ensemble of data from well-calibrated ground stations *McPeters et al.* [2008]. An alternate retrieval of OMI columns, OMDOAO3 [*Veefkind et al.*, 2006] is also available. Use of this product, as well as later versions of the OMTO3 retrievals, would likely have some impacts on the assimilated ozone fields, but will not impact the main conclusions of this study. Ozone profile retrievals (Version 1.5) between 215–0.14 hPa from MLS [*Froidevaux et al.*, 2006; *Waters et al.*, 2006] constrain the profile shape in the upper troposphere, stratosphere and lower mesosphere. In the UTLS, retrievals are provided at 215, 146, 100, and 68 hPa, with a vertical resolution of about 3 km, which is somewhat coarser than that of the model. As in the work of *Stajner et al.* [2008], diagonal elements of the observation error covariances are obtained from the profile precision estimates provided with the retrievals and nondiagonal elements are assumed to be zero. Newer versions of the retrieved Aura data are available. For the MLS ozone the newer V2.2 retrievals are close to the V1.5 retrievals in the region of interest. The largest differences between the two versions are in the mesosphere and in the tropical upper troposphere [*Froidevaux et al.*, 2008]. Experiments show that the main conclusions of this study are not sensitive to changing between V1.5 and V2.2 of the MLS data.

[9] *Stajner et al.* [2008] extensively validated the assimilated ozone against independent data, concentrating mainly on stratospheric profiles and tropospheric partial columns. They found that the assimilated ozone in the lower stratosphere agrees within 10% of independent sonde and aircraft observation. The relative root mean square (RMS) difference with integrated 200–1 hPa ozone columns from SAGE II is within 5%. They also found that tropospheric ozone in the assimilation was more realistic than in the model simulation, with smaller RMS differences from sonde data.

2.2. A Case Study Contrasting Modeled and Assimilated UTLS Ozone

[10] This discussion of the results begins with a comparison of the morphology of modeled and assimilated ozone fields. Visual comparison of ozone maps generated by the model and those from the DAS indicate that spatial structures are very similar in the simulated and assimilated fields, even though the mixing ratios are changed by the assimilation. In particular, the shapes and locations of air mass boundaries, filaments, and local maxima and minima in the assimilation are typically already present in the fields generated by the model. One such comparison is now discussed.

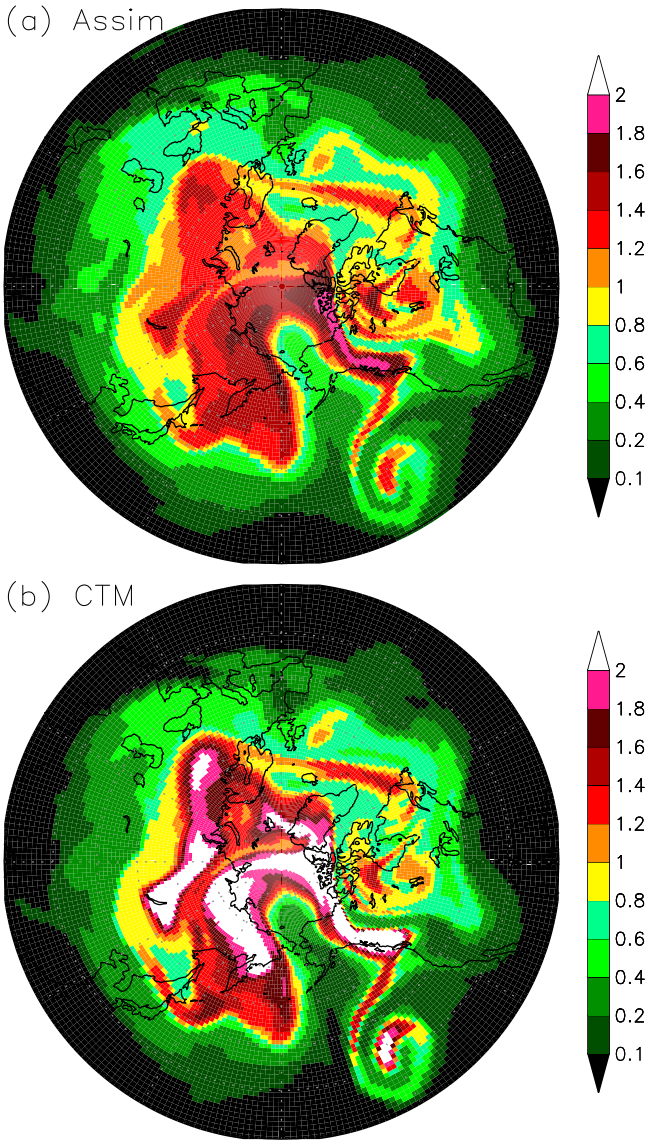

Figure 1. Ozone mixing ratio (ppmv) at 118.25 hPa on 16 March 2005, 6 UTC from (a) assimilation of MLS and OMI ozone into the CCM and (b) the model simulation.

[11] Figure 1 shows ozone at 118.25 hPa (a model layer) at 6 UTC on 16 March 2005, from assimilation and model. Both panels show a tongue of ozone-rich air extending from Alaska into the mid-Pacific, where it wraps around cyclonically. The feature is the lower part of a filament discussed in detail by *Leblanc et al.* [2006] and *Tripathi et al.* [2006] who show that at higher altitudes (435 K) the filament reaches even further south and passes over the Big Island of Hawaii. The spatial structure of this filament is similar in the two cases, but the maximum ozone concentrations are lower in the assimilation than in the model. Features inside the polar vortex reveal a similar discrepancy. A scatterplot of assimilated versus modeled ozone mixing ratios at the model level of 118.25 hPa (Figure 2) gives a more quantitative demonstration of the biases at both low and high concentrations. Compared to the assimilation, the modeled ozone is systematically high biased at mixing ratios larger than about 1 ppmv (part per million by volume), which are typical of the polar vortex at this level, and low biased at the lower mixing ratios typical of midlatitude air masses.

[12] A transect through the fields (Figure 3) shows the longitudinal structure of modeled and assimilated ozone mixing ratios at 40°N and 118.25 hPa on 16 March 2005. The "Hawaiian filament" is seen as a sharp peak between 150°W and 160°W. Figure 1 shows that very similar features appear in both modeled and assimilated fields and Figure 2 shows how the bias in concentrations varies with concentration. Figure 3 shows the impacts of these two effects on the comparison between modeled and assimilated ozone, with both fields showing very similar peaks and troughs, but rather different ranking of the relative strengths of these features (examples are the two double peaks near 60°W and 100°W, where in each case the larger local peak in the assimilated field is the smaller peak in the modeled field).

2.3. Monthly Characterization of Global Structure

[13] The above case study illustrates that differential transport of air masses appears to determine the morphology of the horizontal ozone field in both model and assimilation, while the assimilation acts to change the ozone concentrations within that structure.

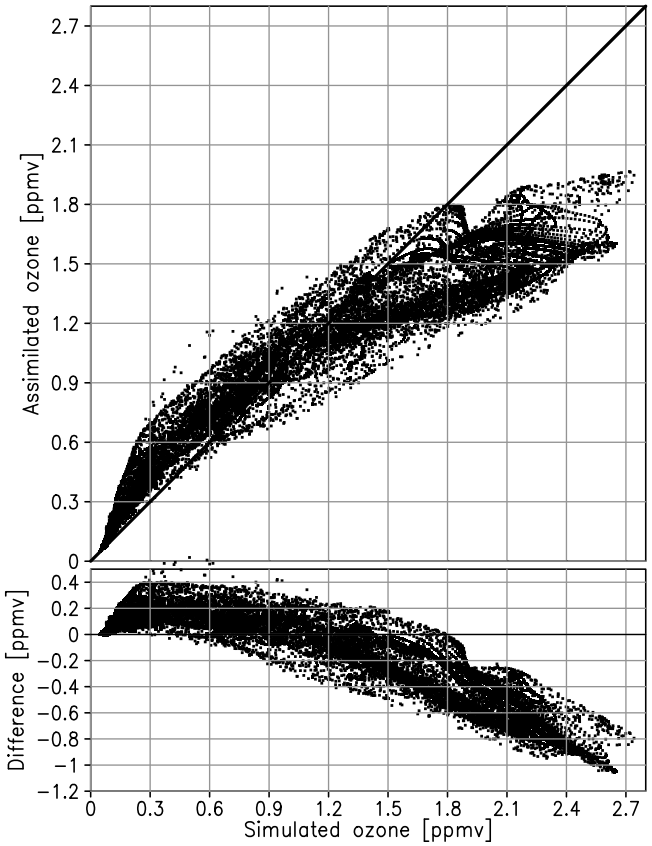

Figure 2. Scatterplots of simulated ozone versus assimilated ozone and simulated ozone versus the difference field at 118.25 hPa on 16 March 2005, 6 UTC. Data from the entire Northern Hemisphere are plotted, and the units are ppmv. Negative values in the difference field are where simulated concentrations exceed those in the assimilation.

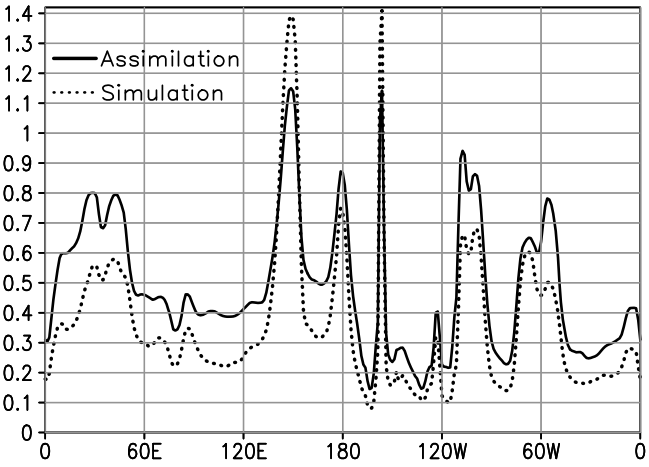

Figure 3. Ozone mixing ratio as a function of longitude at 118.25 hPa at 40°N on 16 March 2005, 6 UTC from assimilation (solid) and simulation (dashed).

[14] This result is now examined in the more general context of accumulated monthly data. Figure 4a shows the histograms with binning at intervals of 0.1 ppmv, of modeled and assimilated ozone at 55°N on the 325 K isentrope in February 2005. Both distributions are bimodal, but have different higher modes and slightly different modal frequencies. At low mixing ratios, typical of tropospheric air, the model has a slightly smaller population near the lower mode of 0.6 ppmv, indicating that the assimilation is constrained to a more uniform upper tropospheric ozone distribution than the simulated ozone. In the stratospheric air masses the assimilated mode (near 0.18 ppmv) is lower and more populated than the modeled mode (0.23 ppmv). The fact that the model (which uses assimilated winds) overestimates the population in the high end of the mixing ratio tail is consistent with excessive transport from higher levels (where ozone abundance is greater). This transport deficiency, which has been noted for several assimilated data sets by *Schoeberl et al.* [2003] and discussed for GEOS-4 by *Pawson et al.* [2007], causes the overestimation of ozone in the model that is corrected by the assimilation process.

[15] A number of prior studies have used trace-gas power spectra to investigate atmospheric variability at a range of spatial scales [e.g., *Strahan and Mahlman*, 1994; *Koshyk et al.*, 1999]. In this study the power $P(k)$ at wave number k of a data series u_0, u_1, … u_{N-1} is computed as $P(k) = ([Fu]_k)^2$, where the Fast Fourier Transform operator, F, is given by

$$[Fu]_k = \frac{1}{N}\sum_{s=0}^{N-1} u_s \exp(-2\pi iks/N).$$

The quantity $P(k)$ represents a measure of variability in the data at the spatial scales determined by k. In general, it is expected that a tracer (or dynamical) field will exhibit scale invariance within a range of scales, so that its power spectrum satisfies a power law, $P(k) \sim k^{\beta}$. The *slope*, β can be thought of as a measure of "smoothness" of the field, with $\beta < -2$ for continuous fields and $\beta = -2$ for data with a finite number of step-like discontinuities. An extreme case is that of white noise which yields $\beta = 0$. All power spectra discussed here are averaged over a month and displayed for wave numbers $k = 1, 2, \ldots N/2$.

[16] Figure 4b shows the monthly ozone power spectra for the ozone fields whose histograms are shown in Figure 4a. The slopes (β) of the modeled and assimilated ozone data are nearly identical, with the spectra differing by a factor that is independent of wave number. The smaller separation of modes in the histogram of the assimilated ozone (Figures 4a and 2) leads to the lower power in that spectrum.

[17] In order to understand contributions of transport and assimilation to different spectral scales, the power spectra of the analysis and transport increments in the assimilation system are discussed. The analysis increments (A(t) − B(t)) are defined as the difference between the 3 h forecasts (backgrounds, B(t)) and the resultant analyses (A(t)) for each analysis time t (every 3 h). Power spectra of (A(t) − B(t)) reveal a steady decrease at the smallest wave numbers (longest zonal waves) and then a relatively rapid spectral decay for wave numbers larger than six (Figure 5). The power spectra of (A(t) − B(t)) in Figure 5 are computed from eight daily sets of A − B on each day in January 2005. The spectral structure of the power in analysis increments can be contrasted with that of the model-evolved fields, computed from the temporal change in ozone (B(t + 3 h) − A(t)) in each 3 h forecast window. Because chemistry is approximated by slow production rates and loss frequencies in this region, these increments are predominantly caused by transport and are referred to as "transport increments." Figure 5 shows that, at the lowest wave numbers, the transport increments are about an order of magnitude larger than the analysis increments, and that $P(k)$ decreases much more slowly for the transport: the spectrum is almost flat up to wave number 10. By wave number 10, the power of the

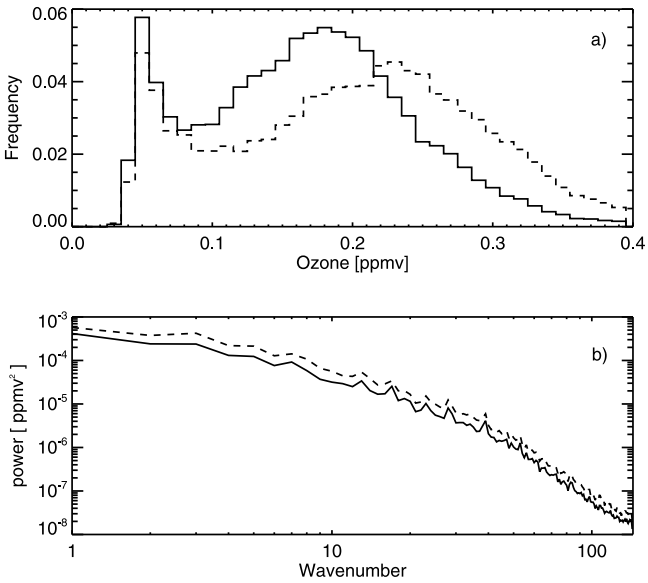

Figure 4. (a) Histograms of the ozone mixing ratio at 55°N on the 325 K isentrope from the model (dashed line) and assimilation (solid line) in February 2005. (b) The spatial power spectrum of the ozone distribution in Figure 4a; wave number 1 corresponds to the longest planetary wave in this plot.

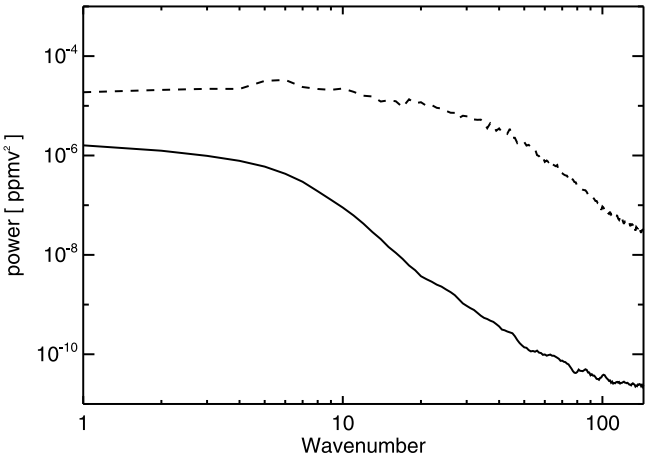

Figure 5. The spatial power spectra of the gridded ozone tendencies in the assimilation computed from transport (dashed line) and analysis increments (solid line), accumulated for January 2005. Data are from 55°N on the 225 hPa model level.

transport increments is about 2 orders of magnitude larger than the analysis increments. These results show that the spatial structure in the assimilated ozone fields is dominated by transport and not by the analysis. Despite the smaller scale of the observations and the small length scales (L = 250 km: *Stajner et al.* [2001]) in the analysis, the spectral power of the increments is concentrated at the largest spectral scales, with only very small corrections to the spatial structure of the ozone field at higher wave numbers. This result is quite insensitive to the length scale assumed: this is discussed further in section 3 in the context of comparison with in situ data.

3. Evaluation With MOZAIC Data

3.1. Data Description

[18] The evaluation in this part of the study includes comparisons with the in situ ozone observations from the Measurement of Ozone and Water Vapor by Airbus In-service Aircraft (MOZAIC) program [*Marenco et al.*, 1998; *Thouret et al.*, 1998] (see also http://mozaic.aero.obs-mip.fr/web/ for more recent information). The MOZAIC sensors, mounted on five commercial aircraft, measure ozone every 4 s, which corresponds to a spatial resolution of about 1 km. Most MOZAIC flights are in the Northern Hemisphere between Europe and North America, but some are between Europe and Asia or Southern Africa. The typical pressure at cruising altitude is in the range of 263–215 hPa, which provides observations in both the upper troposphere and the lower stratosphere as the planes repeatedly cross the tropopause. MOZAIC observations have been used to document UTLS ozone structure [e.g., *Thouret et al.*, 2006; *Bortz et al.*, 2006], to demonstrate their relationship with meteorological features [e.g., *Cooper et al.*, 2006] as well as to study long-term trends in the UTLS ozone concentrations [*Schnadt Poberaj et al.*, 2009].

[19] Expanding on the work of *Stajner et al.* [2008], MOZAIC data are used as an estimate of the true state of the ozone distribution against which the modeled and assimilated ozone are validated. The analysis uses data from altitudes higher than 8 km, omitting the information obtained during take-off and landing, and the remaining data are averaged over flight segments within each 1° × 1.25° grid box of the GCM. To enable direct comparisons with the observations, the modeled and assimilated fields are interpolated to the locations of the appropriate flight segment centers. The interpolation is bilinear in the horizontal, linear in log-pressure and linear in time.

[20] Figure 6a shows time series of the monthly root mean square (RMS) differences between the interpolated assimilated and modeled ozone and all available MOZAIC data in 2005. The closer agreement of the assimilated ozone with MOZAIC data, especially in January–June 2005, shows that the impacts of assimilation (Figures 1–4) represent improvements compared to the model. Through 2005, there is a pronounced change in the agreement between the GEOS assimilation and the observations: RMS differences are near 0.05–0.06 ppmv in the first half of the year and decrease to

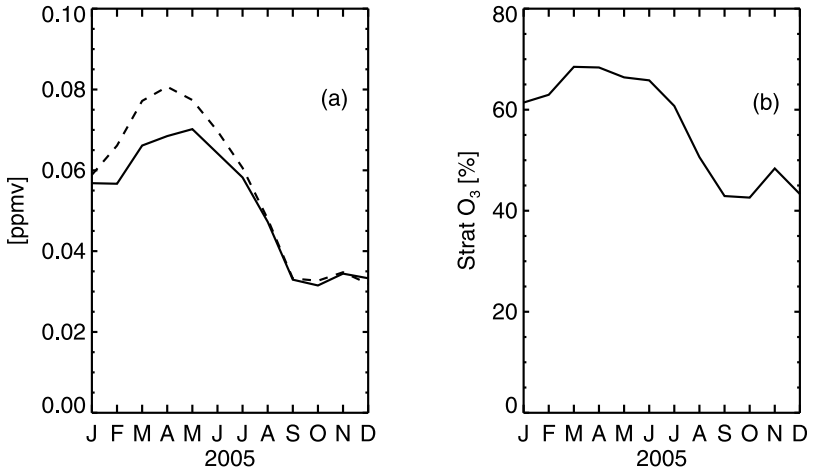

Figure 6. (a) Time series of monthly RMS difference between all available MOZAIC ozone data (interpolated to the 1° × 1.25° model grid) and the simulated (dashed) and assimilated (solid) ozone fields. (b) Percentage of measured MOZAIC ozone in excess of 0.1 ppmv for each month: such concentrations represent stratospheric air.

values as low as 0.03 ppmv near the end of the year. The RMS difference for the model run relative to the measured ozone (not shown) changes from ~34% in January 2005 to 26% in December 2005. Those month-to-month differences can likely be attributed to a sampling pattern in which most observations were made in the stratosphere in January–June and in the troposphere in July–December. Figure 6b shows the percentage of MOZAIC ozone observations in each month that exceed 0.1 ppmv, which is an approximate threshold. For the first 6 months of 2005 over 60% of sampled air was ozone-rich, indicative of stratospheric air. The fraction decreases to 40%–46% in October–December. The largest improvement exhibited by assimilation over model (over 0.01 ppmv) is seen in March and April and coincides with the maximum percentage of stratospheric ozone sampled by the aircraft in that period (over 68%). Spatial distributions of MOZAIC ozone concentrations at 238 hPa for January and December 2005 (Figure 7) highlight several aspects of the observations. First, in the later month more of the MOZAIC flights crossed the Tropics, where flight altitudes are usually in the troposphere: none of the aircraft carrying MOZAIC instruments flew to South America or South Africa in January. Second, flights into Japan encountered generally lower ozone concentrations at 238 hPa in December 2005 than in January 2005. Third, even though the majority of flight tracks in both months covered the North Atlantic and North America, the observations in December sampled lower ozone concentrations than those in January. Fourth, the only flight paths with substantially low ozone concentrations in January were on routes between Europe and Florida. The following discussion concentrates on January and February when the majority of the flight tracks were in the 40°–80°N latitude range.

3.2. Comparisons of Spatial Scales

[21] The main objective here is to statistically evaluate spatial scales in the assimilated data using the aircraft observations. Monthly averaged ozone power spectra from the MOZAIC data and from the corresponding interpolated model and assimilation are compared. They were computed as follows. Grid-averaged data from each flight were truncated to a segment covering the first 50 model grid cells (approximately 5000 km on the 1.25° grid in middle latitudes), after which the power spectra for wave numbers $k = 1$ to 25 were computed; the average power spectrum for the entire month was derived from these individual records. (Note that these wave numbers are different from those computed on the regular longitudinal grid in section 2.) Figure 8a shows the power spectra from the MOZAIC data ($P_{ob}(k)$) and from the modeled ($P_m(k)$) and assimilated ozone ($P_a(k)$) data after interpolation to the MOZAIC flight tracks. As for the ozone data on the model grid (Figure 4), the ratio $P_a(k)/P_m(k)$ varies only weakly with wave number, ranging from 0.6 to 0.7 (Figure 8b), indicating only very small changes in spatial structure between these two data sets. There is a distinct change in the relationship between the MOZAIC observations and the other data sets, with $P_{ob}(k)/P_m(k)$ changing from about 0.7 to values in excess of 1.5 near $k = 8$. (This roughly corresponds to a wavelength of about 600 km.)

[22] Two broad aspects of these results remain true in all months of 2005: the ratio $P_a(k)/P_m(k)$ is almost independent of k and $P_{ob}(k)$) is flatter than other spectra, with more power at larger k. This shows that both the simulation and the assimilation are representing spatial scales with $k < 8$, or about six model grid boxes, more realistically than shorter scales.

3.3. Sensitivity to Details of the Assimilation

[23] Small-scale variability in assimilated fields is potentially influenced by the choice of background error covariance structure as it controls the spatial distribution of analysis increments. In this ozone assimilation [*Stajner et al.*, 2001], the background error variance for ozone is proportional to the forecasted mixing ratio, with a proportionality coefficient, α, and the background error correlation is controlled by the characteristic length scale, L. The sensitivity of the spectral slope to the choice of the tunable parameters, L and α has been examined.

[24] In order to quantify the impact of correlation length scale, two additional experiments in which L was set to 150 and 400 km, bracketing the main experiment's 250 km length, were performed. As expected the power spectra flatten slightly at large wave numbers for the $L = 150$ km run, but the overall difference between the spatial power spectra in the two perturbation experiments is within 2% of the control. This impact is small compared to the differences shown in Figure 8.

[25] The sensitivity of the spectral slope to the choice of the parameter α is shown in Figure 9. In addition to the main assimilation experiment with $\alpha = 0.3E - 4$, we performed another experiment increasing the parameter by a factor of 5 and hence indirectly increasing the magnitude of analysis increments. The plot shows the ratio of the power spectra of the MOZAIC data and the two assimilation experiments to that in the simulation, for January 2005. It is clear that increasing forecast error variances and consequently the magnitude of analysis increments, which could feasibly increase the local impact of the assimilation and hence generate more localized features, has almost no impact on the wave number dependence of power, even though stronger reliance on observations increases the power across all wave numbers.

3.4. Power Spectra of Smoothed MOZAIC Data

[26] In order to investigate how strongly the aircraft data need to be smoothed in order to reduce their small-scale variability to that of the model/assimilation, the following binomial smoothing scheme was applied to the MOZAIC data:

$$\overline{\mu(k)} = \frac{1}{2^n}\sum_{s=0}^{n} C_s^n \mu(k - n/2 + s),$$

where $\mu(1)$, $\mu(2)$,…, $\mu(k)$,… represent the (averaged) aircraft data, n is a parameter, and C_s^n is a binomial coefficient [*Marchand and Marmet*, 1983]. This smoothing procedure is roughly equivalent to integrating the data with a Gaussian kernel. It introduces autocorrelation into the data with a length scale controlled by the parameter n, here assumed to be an even positive integer. The smoothing was applied for $n = 2$, 4, 6, and 8, where $n = 2$ corresponds to a 1-2-1

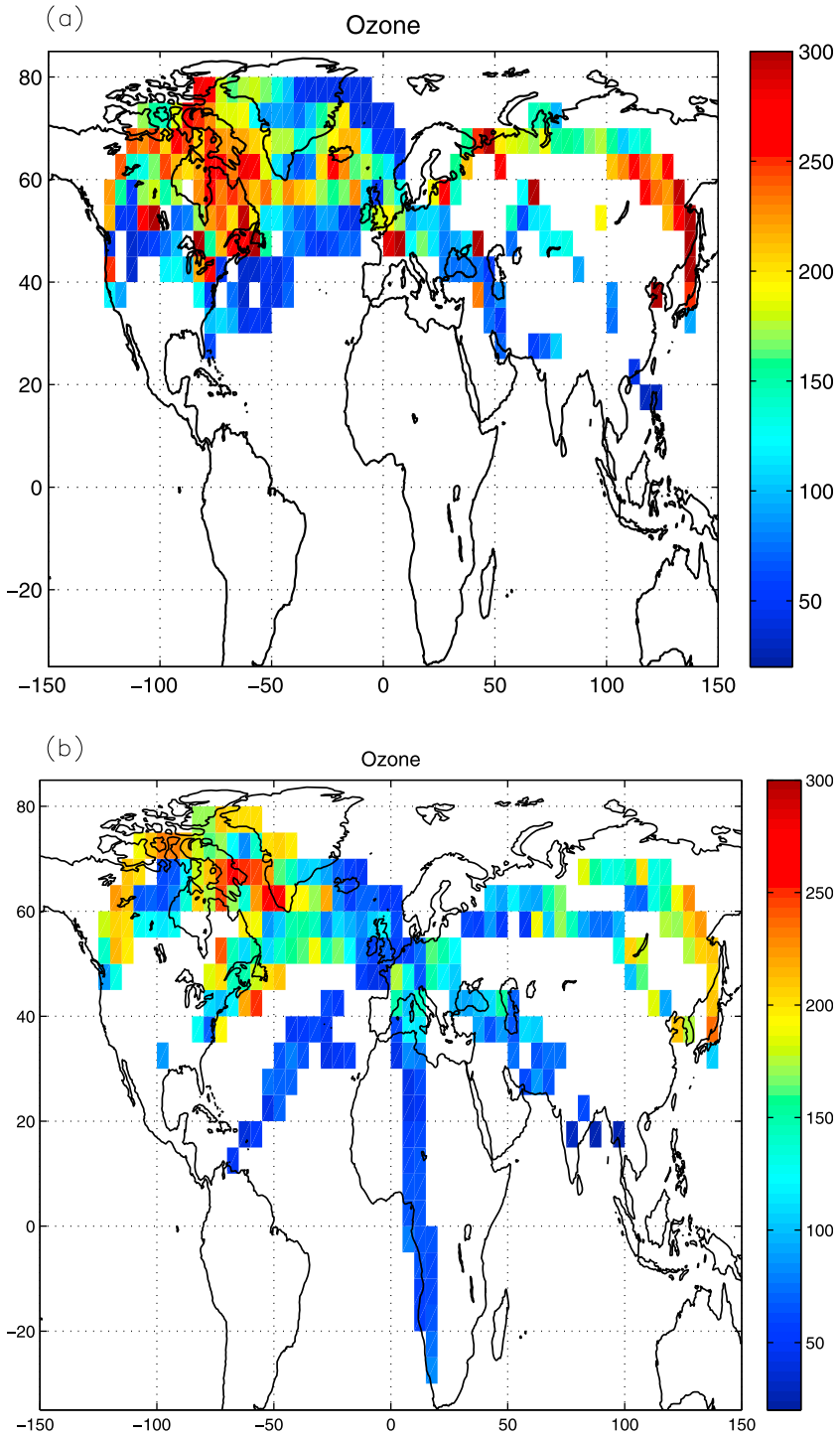

Figure 7. Ozone concentrations (ppbv) composited from MOZAIC observations at 238 hPa in (a) January 2005 and (b) December 2005. Low concentrations, denoted by blue shades, represent tropospheric air. The geographical distribution of data reflects the flight paths of the aircraft carrying the MOZAIC instrumentation.

smoother over three grid boxes. The MOZAIC power spectra were recalculated for each of these smoothing values. Figure 10 shows $P_{ob}(k)/P_m(k)$ for different levels of smoothing (n = 0 means no smoothing at all). As expected, the spatial smoothing has the largest impact on higher wave numbers, with stronger reduction in MOZAIC power as the order of smoothing is increased. Smoothing over 5 (n = 4) or 7 (n = 6) grid boxes brings the aircraft to model power ratio the closest to a constant in this case. This shows that the spatial power spectra of the modeled and assimilated ozone

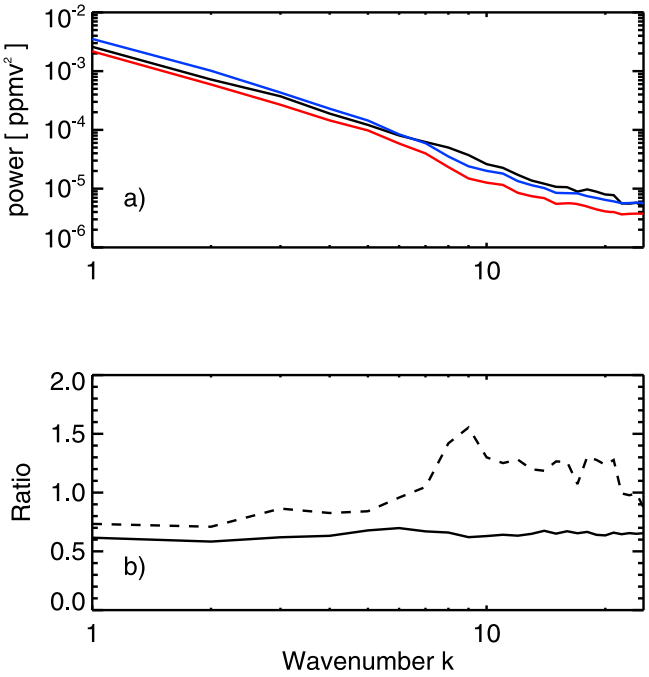

Figure 8. (a) Ozone power spectra in February 2005 calculated on MOZAIC flight tracks from MOZAIC data (black), the model (blue), and assimilation (red). (b) The ratio of the power from assimilation to model (solid) and MOZAIC to model (dashed). Note that the wave number in Figures 8–10 refers to a 50 box segment of the MOZAIC flight track interpolated to the model grid and not to the complete latitude circles used in Figures 4b and 5.

fields are similar to the gridded MOZAIC data when these are spatially smoothed to resolve features with scales of 4–6 grid boxes. Additionally, this supports the notion that the assimilation (like the model) does not resolve features with spatial scales of less than about six grid boxes.

4. Summary and Discussion

[27] Assimilation studies, including *Jackson* [2007] and *Stajner et al.* [2008], have demonstrated benefits of assimilation of MLS data for representation of ozone in the UTLS. The successive increases in realism of lower-stratospheric ozone when assimilating space-based observations is highlighted using Michelson Interferometer for Passive Atmospheric Sounding (MIPAS) [*Wargan et al.*, 2005] and the MLS ozone [*Stajner et al.*, 2008]. The good general agreement between assimilated MLS ozone and MOZAIC data indicate the strong potential of such observations for helping constrain radiative forcing of climate by UTLS ozone and for providing important knowledge of UTLS ozone distributions for the context of stratosphere-troposphere exchange, long-range pollution transport and air-quality forecasting. This indicates the need for long-term observations of UTLS ozone from space using observing techniques that provide adequate spatial coverage to constrain UTLS ozone.

[28] This study has presented a detailed evaluation of hitherto unexplored aspects of assimilated UTLS ozone, focusing on similarities and differences in spatial power spectra in simulated and assimilated ozone and additional comparison with observations.

[29] The ability of large-scale flows to deform and produce much smaller structures in tracers is well known [e.g., *Shepherd et al.*, 2000]. The importance of the numerical transport code, including advection and diffusion, in determining the horizontal scales that are represented is also well known [e.g., *Koshyk et al.*, 1999]. *Lin and Rood* [1996] used their advection scheme to transport a step function in a 50 cell one-dimensional domain. In their example, the initial discontinuity becomes spread over six grid cell lengths, describing an effective limit to the finest scales represented in a model of finite resolution. Our finding that the MOZAIC data must be smoothed over four to six model grid-boxes to yield power spectra that are similar to those in the modeled and assimilated ozone fields are consistent with the Lin-Rood experiments. This means that the effective resolution of these "1° × 1.25°" ozone simulations and analyses is about 6° × 7.5°, due to suppression of variability at the finest scales. This paper has shown that this fundamental property of the transport is unaffected by assimilation: that is, assimilation did not add fine-scale structure to the ozone fields.

[30] Because analysis increments are applied on spatial scales of several hundred kilometers, we may anticipate that the power spectra of the assimilated ozone will differ from that of the modeled ozone at those wavelengths. This is not the case. Instead, the results show that spectral power of analysis increments is concentrated at long spatial scales. The assimilation thus constrains ozone concentrations in the largest pools, most notably decreasing the high bias often seen in ozone simulations in the extratropical lower stratosphere that is predominantly due to overstrong Brewer-Dobson circulation when using assimilated winds [e.g., *Douglass et al.*, 1996]. The spectral cascade of power from longer to shorter wavelengths controls the ozone power

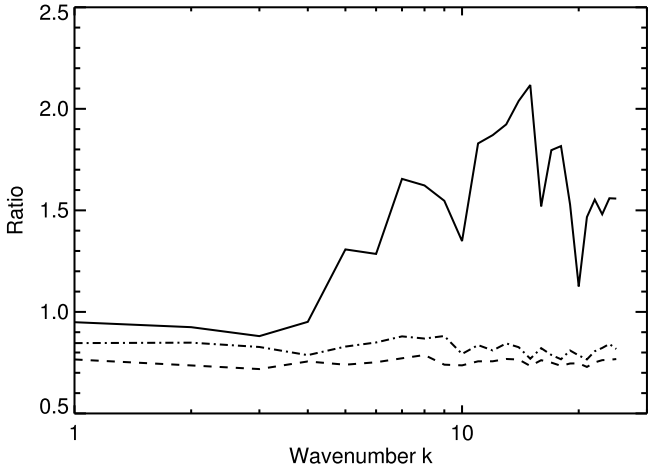

Figure 9. Ratios of ozone power spectra to those in the model simulation for MOZAIC observations (solid) and two assimilation experiments, with $\alpha = 0.3E - 4$ (dashed) and $\alpha = 1.5E - 4$ (dot-dashed). The parameter α is the constant of proportionality between the background error and the forecasted ozone concentration [*Stajner et al.*, 2001]. Results are for January 2005.

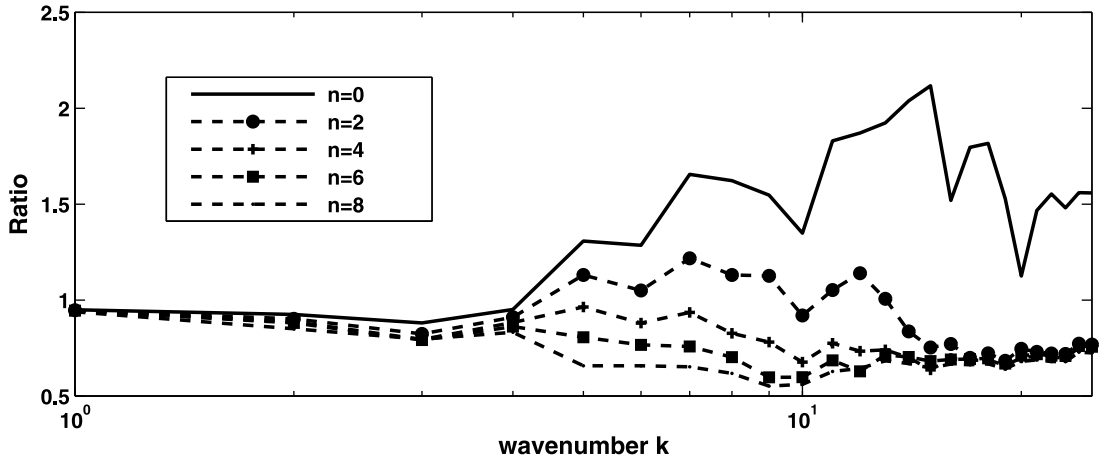

Figure 10. The impact of smoothing the MOZAIC data on the ratios of power spectra. The ratios between spectral power in MOZAIC data to that in the simulation are shown for January 2005. The solid curve, with $n = 0$, is identical to the solid curve in Figure 9. Details on the smoothing parameter n are given in section 3.4.

spectrum in the assimilation, just as it does in the model. Evaluation of increments showed this cascade in transport tendencies, in contrast with the sharp reduction in power of analysis increments after the longest spatial scales. This implies that even though the individual analysis increments are applied at shorter scales, the spatial organization of these increments results in a cumulative impact at larger spatial scales.

[31] To our knowledge, this is the first time such behavior has been examined in a trace-gas assimilation scheme. *Tanguay et al.* [1995] investigated the ability of an assimilation system to transfer information from larger to smaller scales in the context of the evolution by the adjoint of a nonlinear model in four-dimensional variational assimilation. They also found that model fidelity is the key for small scales: the transfer of information to small scales was limited when linearization of the model was no longer appropriate and that relative errors were largest at small scales.

[32] In summary, we have demonstrated that the assimilation of UTLS ozone acts primarily on the largest scales to constrain "pools" of ozone, tending to correct the systematic errors in the transport circulation discussed by *Tan et al.* [2004]. The downscaling cascading supported by the *Lin and Rood* [1996] transport scheme serves to maintain resolution of structures down to about the four-to-six model grid box scale: about six degrees in this one-degree system. Spectral power of the analysis increments does not add substantial structure at the scales of the correlation lengths used in the assimilation, implying that the increments are spatially organized in the assimilation system presented here.

[33] **Acknowledgments.** We appreciate the support from and discussions with our colleagues Eric Nielsen and Andrew Tangborn. We are grateful to Nathaniel Livesey and Lucien Froidevaux of the MLS Scence Team at NASA's JPL and to Pieternel Levelt at KNMI for discussions about the MLS and the Dutch-Finnish OMI data. Comments by three anonymous reviewers and the Associate Editor substantially improved the presentation of our results. The research was funded by NASA's Atmospheric Chemistry Modeling and Analysis Program (ACMAP). Computing resources were provided by NASA's High-Performance Computing program. We acknowledge the strong support of the European Commission, Airbus, and the airlines (Lufthansa, Austrian, Air France), who have carried and maintained the MOZAIC equipment, free of charge, since 1994. MOZAIC is presently funded by INSU-CNRS (France), Météo-France, and Forschungszentrum Jülich (FZJ) Germany. The MOZAIC database is supported by ETHER (CNES and INSU-CNRS).

References

Bhartia, P. K., and C. W. Wellemeyer (2002), OMI TOMS-V8 Total O3 Algorithm, in *Algorithm Theoretical Baseline Document: OMI Ozone Products, ATBD-OMI-02*, version 2.0, vol. II, edited by P. K. Bhartia, pp. 15–31, NASA GSFC, Greenbelt, Md. (Available at http://eospso.gsfc.nasa.gov/eos_homepage/for_scientists/atbd/docs/OMI/ATBD-OMI-02.pdf)

Bloom, S. C., et al. (2005), *The Goddard Earth Observing System Data Assimilation System, GEOS DAS Version 4.0.3: Documentation and Validation*, *Tech. Rep. Ser. on Global Model. and Data Assimil. 104606*, 26, 181 pp., NASA Goddard Space Flight Cent., Greenbelt, Md.

Bortz, S. E., M. J. Prather, J.-P. Cammas, V. Thouret, and H. Smit (2006), Ozone, water vapor, and temperature in the upper tropical troposphere: Variations over a decade of MOZAIC measurements, *J. Geophys. Res.*, *111*, D05305, doi:10.1029/2005JD006512.

Cooper, O. R., et al. (2006), Large upper tropospheric ozone enhancements above midlatitude North America during summer: In situ evidence from the IONS and MOZAIC ozone measurement network, *J. Geophys. Res.*, *111*, D24S05, doi:10.1029/2006JD007306.

de Laat, A. T. J., R. J. van der A, and M. van Weele (2009), Evaluation of tropospheric ozone columns derived from assimilated GOME ozone profile observations, *Atmos. Chem. Phys.*, *9*, 8105–8120, doi:10.5194/acp-9-8105-2009.

Douglass, A. R., C. J. Weaver, R. B. Rood, and L. Coy (1996), A three-dimensional simulation of the ozone annual cycle using winds from a data assimilation system, *J. Geophys. Res.*, *101*(D1), 1463–1474, doi:10.1029/95JD02601.

Feng, L., R. Brugge, E. V. Holm, R. S. Harwood, A. O'Neill, M. J. Filipiak, L. Froidevaux, and N. Livesey (2008), Four-dimensional variational assimilation of ozone profiles from the Microwave Limb Sounder on the Aura satellite, *J. Geophys. Res.*, *113*, D15S07, doi:10.1029/2007JD009121.

Froidevaux, L., et al. (2006), Early validation analyses of atmospheric profiles from EOS MLS on the Aura satellite, *IEEE Trans. Geosci. Remote Sens.*, *44*, 1106–1121, doi:10.1109/TGRS.2006.864366.

Froidevaux, L., et al. (2008), Validation of Aura Microwave Limb Sounder stratospheric ozone measurements, *J. Geophys. Res.*, *113*, D15S20, doi:10.1029/2007JD008771.

Hudman, R. C., et al. (2007), Surface and lightning sources of nitrogen oxides over the United States: Magnitudes, chemical evolution, and outflow, *J. Geophys. Res.*, *112*, D12S05, doi:10.1029/2006JD007912.

Jackson, D. R. (2007), Assimilation of EOS MLS ozone observations in the Met Office data-assimilation system, *Q. J. R. Meteorol. Soc.*, *133*, 1771–1788, doi:10.1002/qj.140.

Koshyk, J., B. Boville, K. Hamilton, E. Manzini, and K. Shibata (1999), Kinetic energy spectrum of horizontal motions in middle-atmosphere models, *J. Geophys. Res.*, *104*(D22), 27,177–27,190, doi:10.1029/1999JD900814.

Leblanc, T., O. P. Tripathi, I. S. McDermid, L. Froidevaux, N. J. Livesey, W. G. Read, and J. W. Waters (2006), Simultaneous lidar and EOS MLS measurements, and modeling, of a rare polar ozone filament event over Mauna Loa Observatory, Hawaii, *Geophys. Res. Lett.*, *33*, L16801, doi:10.1029/2006GL026257.

Levelt, P. F., et al. (2006), The Ozone Monitoring Instrument, *IEEE Trans. Geosci. Remote Sens.*, *44*(5), 1093–1101, doi:10.1109/TGRS.2006.872333.

Lin, S.-J., and R. B. Rood (1996), Multidimensional flux-form semi-Langrangian transport schemes, *Mon. Weather Rev.*, *124*, 2046–2070, doi:10.1175/1520-0493(1996)124<2046:MFFSLT>2.0.CO;2.

Marchand, L., and L. Marmet (1983), Binomial Smoothing Filter: A way to avoid some pitfalls of least squares polynomial smoothing, *Rev. Sci. Instrum.*, *54*(8), 1034–1041, doi:10.1063/1.1137498.

Marenco, A., et al. (1998), Measurement of ozone and water vapor by Airbus in-service aircraft: The MOZAIC airborne program, An overview, *J. Geophys. Res.*, *103*(D19), 25,631–25,642, doi:10.1029/98JD00977.

McPeters, R. D., G. J. Labow, and J. A. Logan (2007), Ozone climatological profiles for satellite retrieval algorithms, *J. Geophys. Res.*, *112*, D05308, doi:10.1029/2005JD006823.

McPeters, R., M. Kroon, G. Labow, E. Brinksma, D. Balis, I. Petropavlovskikh, J. P. Veefkind, P. K. Bhartia, and P. F. Levelt (2008), Validation of the Aura Ozone Monitoring Instrument total column ozone product, *J. Geophys. Res.*, *113*, D15S14, doi:10.1029/2007JD008802.

Parrington, M., D. B. A. Jones, K. W. Bowman, L. W. Horowitz, A. M. Thompson, D. W. Tarasick, and J. C. Witte (2008), Estimating the summertime tropospheric ozone distribution over North America through assimilation of observations from the Tropospheric Emission Spectrometer, *J. Geophys. Res.*, *113*, D18307, doi:10.1029/2007JD009341.

Pawson, S., I. Stajner, S. R. Kawa, H. Hayashi, W.-W. Tan, J. E. Nielsen, Z. Zhu, L.-P. Chang, and N. J. Livesey (2007), Stratospheric transport using 6-h-averaged winds from a data assimilation system, *J. Geophys. Res.*, *112*, D23103, doi:10.1029/2006JD007673.

Pierce, R. B., et al. (2007), Chemical data assimilation estimates of continental U.S. ozone and nitrogen budgets during the Intercontinental Chemical Transport Experiment: North America, *J. Geophys. Res.*, *112*, D12S21, doi:10.1029/2006JD007722.

Schnadt Poberaj, C., J. Staehelin, D. Brunner, V. Thouret, H. De Backer, and R. Stübi (2009), Long-term changes in UT/LS ozone between the late 1970s and the 1990s deduced from the GASP and MOZAIC aircraft programs and from ozonesondes, *Atmos. Chem. Phys.*, *9*, 5343–5369, doi:10.5194/acp-9-5343-2009.

Schoeberl, M. R., A. R. Douglass, Z. Zhu, and S. Pawson (2003), A Comparison of the lower stratospheric age spectra derived from a general circulation model and two data assimilation systems, *J. Geophys. Res.*, *108*(D3), 4113, doi:10.1029/2002JD002652.

Semane, N., V.-H. Peuch, L. El Amraoui, H. Bencherif, S. Massart, D. Cariolle, J.-L. Attié, and R. Abida (2007), An observed and analysed stratospheric ozone intrusion over the high Canadian Arctic UTLS region during the summer of 2003, *Q. J. R. Meteorol. Soc.*, *133*(S2), 171–178, doi:10.1002/qj.141.

Shepherd, T. G., J. Koshyk, and K. Ngan (2000), On the nature of large-scale mixing in the stratosphere and mesosphere, *J. Geophys. Res.*, *105*(D10), 12,433–12,446, doi:10.1029/2000JD900133.

Stajner, I., and K. Wargan (2004), Antarctic stratospheric ozone from the assimilation of occultation data, *Geophys. Res. Lett.*, *31*, L18108, doi:10.1029/2004GL020846.

Stajner, I., L. P. Riishøjgaard, and R. B. Rood (2001), The GEOS ozone data assimilation system: Specification of error statistics, *Q. J. R. Meteorol. Soc.*, *127*, 1069–1094.

Stajner, I., et al. (2008), Assimilated ozone from EOS-Aura: Evaluation of the tropopause region and tropospheric columns, *J. Geophys. Res.*, *113*, D16S32, doi:10.1029/2007JD008863.

Strahan, S. E., and J. D. Mahlman (1994), Evaluation of the SKYHI general circulation model using aircraft N2O measurements: 2. Tracer variability and diabatic meridional circulation, *J. Geophys. Res.*, *99*, 10,319–10,332, doi:10.1029/94JD00044.

Tan, W. W., M. A. Geller, S. Pawson, and A. da Silva (2004), A case study of excessive subtropical transport in the stratosphere of a data assimilation system, *J. Geophys. Res.*, *109*, D11102, doi:10.1029/2003JD004057.

Tanguay, M., P. Bartello, and P. Gauthier (1995), Four-dimensional data assimilation with a wide range of scales, *Tellus, Ser. A*, *47*, 974–997.

Terao, Y., and J. A. Logan (2007), Consistency of time series and trends of stratospheric ozone as seen by ozonesondes, SAGE II, HALOE, and SBUV(/2), *J. Geophys. Res.*, *112*, D06310, doi:10.1029/2006JD007667.

Thouret, V., A. Marenco, J. A. Logan, P. Nédélec, and C. Grouhel (1998), Comparisons of ozone measurements from the MOZAIC airborne program and the ozone sounding network at eight locations, *J. Geophys. Res.*, *103*, 25,695–25,720, doi:10.1029/98JD02243.

Thouret, V., J.-P. Cammas, B. Sauvage, G. Athier, R. Zbinden, P. Nédélec, P. Simon, and F. Karcher (2006), Tropopause referenced ozone climatology and inter-annual variability (1994–2003) from the MOZAIC programme, *Atmos. Chem. Phys.*, *6*, 1033–1051, doi:10.5194/acp-6-1033-2006.

Tripathi, O. P., T. Leblanc, I. S. McDermid, F. Lefèvre, M. Marchand, and A. Hauchecorne (2006), Forecast, measurement, and modeling of an unprecedented polar ozone filament event over Mauna Loa Observatory, Hawaii, *J. Geophys. Res.*, *111*, D20308, doi:10.1029/2006JD007177.

Veefkind, J. P., J. F. de Haan, E. J. Brinksma, M. Kroon, and P. F. Levelt (2006), Total ozone from the Ozone Monitoring Instrument (OMI) Using the DOAS technique, *IEEE Trans. Geosci. Remote Sens.*, *44*(5), 1239–1244, doi:10.1109/TGRS.2006.871204.

Wargan, K., I. Stajner, S. Pawson, R. B. Rood, and W.-W. Tan (2005), Monitoring and assimilation of ozone data from the Michelson interferometer for passive atmospheric sounding, *Q. J. R. Meteorol. Soc.*, *131*, 2713–2734, doi:10.1256/qj.04.184.

Waters, J. W., et al. (2006), The Earth Observing System Microwave Limb Sounder (EOS MLS) on the Aura satellite, *IEEE Trans. Geosci. Remote Sens.*, *44*, 1075–1092, doi:10.1109/TGRS.2006.873771.

S. Pawson, Global Modeling and Assimilation Office, NASA Goddard Space Flight Center, 8463 Greenbelt Rd., Greenbelt, MD 20770-2548, USA. (steven.pawson@nasa.gov)

I. Stajner, Noblis, Inc., 3150 Fairview Park Dr., Falls Church, VA 22042, USA.

V. Thouret, Laboratoire d'Aérologie, UPS, Université de Toulouse, 14 ave. Edouard Belin, F-31400 Toulouse, France.

K. Wargan, Department of Physics, Imperial College London, South Kensington Campus, London SW7 2AZ, UK.